EUROPHYSICS LETTERS 1 June 2002

Europhys. Lett., **58** (5), pp. 737–743 (2002)

X-ray study of the structure and order in lithographic Cu_3Au nano-cuboids

T. Schülli[1](*), J. Trenkler[1], I. Mönch[2], D. Le Bolloc'h[3] and H. Dosch[1]

[1] *Max-Planck Institut für Metallforschung - D-70569 Stuttgart, Germany and Universität Stuttgart, Institut für Theoretische und Angewandte Physik D-70569 Stuttgart, Germany*

[2] *Institut für Festkörper- und Werkstofforschung - D-01069 Dresden, Germany*

[3] *Laboratoire de Physique des Solides, Université Paris Sud 91405 Orsay, France*

(received 21 December 2001; accepted in final form 6 March 2002)

PACS. 68.35.Rh – Phase transitions and critical phenomena.

PACS. 68.65.-k – Low-dimensional, mesoscopic, and nanoscale systems: structure and non-electronic properties.

PACS. 61.10.Eq – X-ray scattering (including small-angle scattering).

Abstract. – We present a structural and thermodynamic study of lithographically produced Cu_3Au nano-structures on a sample which contained both an array of periodically arranged nano-cuboids with a size of $200 \times 200 \times 13$ nm^3 and a closed thin film. It is shown that the coherence features of the X-ray beam and the periodical arrangement of the nano-structures give rise to an unusual interference pattern which is exploited as a control tool for the sample quality during the experiment. With this in hand, the $L1_2$-A_2 phase transformation in the nano-structures is investigated together with the behaviour of the thin film which can be compared *in situ*. The temperature-dependent study at this order-disorder phase transformation yields a remarkable difference in the transition temperature T_c, where T_c of the nano-cuboids is about 200 K lower than in the closed film.

Cooperative phenomena in confined systems are a theoretical and experimental challenge in condensed-matter physics: Of current scientific interest is the interplay between the finite size of the system, the presence of surfaces and external fields and how the resulting structural inhomogeneities affect the thermodynamic and dynamic characteristics of phase transformations. Model systems for structural phase transitions are binary alloys like Cu_3Au, β-CuZn or Fe_3Al which undergo an order-disorder phase transformation. In the past 15 years the influence of surfaces on order-disorder phase transformations has been studied in great detail by theory [1–7] and experiment (see [8] and references in [9]) and new, partly universal, phenomena have been revealed, such as new universal critical exponents [6,7,10], disorder-wetting transitions [11], surface segregation [12] and changed dynamical behaviour [13]. With the recent progress in nano-technology and X-ray scattering (utilizing highly brilliant synchrotron radiation), reproducible experimental studies of order-disorder transformation in binary nano-systems with a tailored confinement are now possible. In this communication, we report a first X-ray diffraction study of lithographically produced Cu_3Au nano-cuboids. We show that the

(*) Present address: European Synchrotron Radiation Facility - BP 220, F-38043 Grenoble Cedex, France.

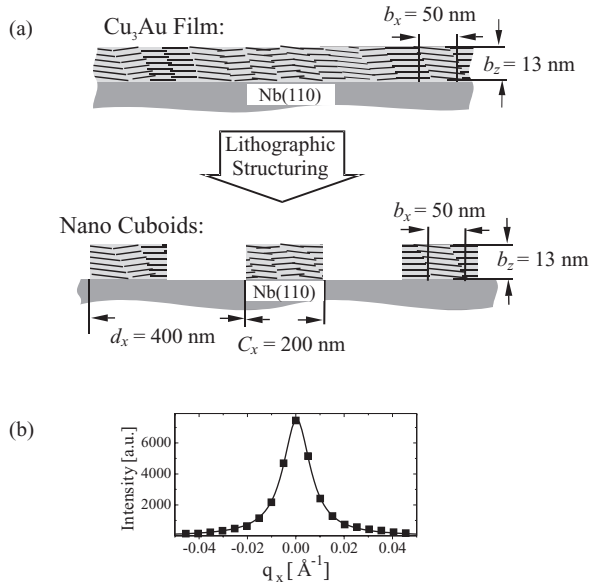

Fig. 1 – (a) Mosaic structure of a thin $Cu_3Au(111)$ film grown on a Nb(110) buffer layer and of the lithographically produced nano-cuboids (note that the aspect ratio is not to scale). (b) Measured Lorentzian intensity distribution of the $Cu_3Au(111)$ reflection associated with the mosaicity of the Cu_3Au film (see text).

partially coherent X-ray beam gives rise to unusual diffraction signals from the arrangement of the nano-cuboids and present a first study of the order-disorder phase transformation within the binary Cu_3Au nano-cuboids revealing a rather unexpected and puzzling thermodynamic behaviour.

Cu_3Au undergoes a discontinuous (first order) transition from the ordered $L1_2$ to the disordered fcc structure at $T_c = 660$ K. The characteristics of this phase transformation have been studied extensively in the bulk [14, 15], at surfaces [12] and in thin films [9, 16]. For our studies, a crystalline Cu_3Au film of 13 nm thickness has been grown epitaxially on a 45 nm single-crystalline Nb(110) buffer layer which is deposited on a high-quality $Al_2O_3(11\overline{2}0)$ substrate as shown schematically in fig. 1(a). The distribution of the mosaic blocks within the film was measured by X-ray rocking scans of the $Cu_3Au(111)$ reflection as in fig. 1(b) and is well described by a Lorentzian (full line),

$$I(q_x) \propto \frac{1}{(w_x^2 + 4q_x^2)}, \tag{1}$$

with a FWHM w_x which corresponds to a mosaic block size of about $b_x = 50$ nm. Cu_3Au nano-cuboids of size $200 \times 200 \times 13$ nm^3 and with a lateral period of 400 nm have been produced by electron lithography on the central 1 mm^2 area of the sample (within a 10×10 mm^2 film). Notice that the sample consists of Cu_3Au nano-cuboids located in the centre of the sample and a closed Cu_3Au film around it. We used a negative photoresist (with a dwell time of 4.5 μs) and a 4.8 keV electron beam to minimize the unwanted proximity effect (backscattering of the electrons which limits the perfection of metal nano-structures). The Cu_3Au nano-cuboids were finally obtained by imprinting the photomask with 1 keV Ar^+ ions under high-vacuum conditions. Figure 2(a) shows a scanning electron microscope image

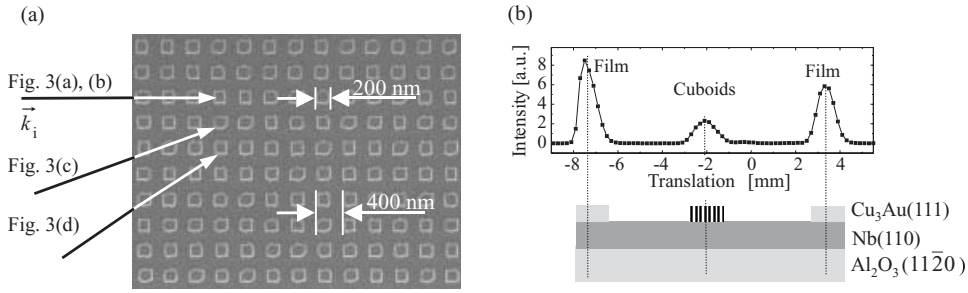

Fig. 2 – (a) SEM image of the periodically arranged $Cu_3Au(111)$ nano-cuboids. The directions of the incident beam for the scans shown in the following figures are indicated by the arrows. (b) Principle of the *in situ* X-ray study of the thin film and the nano-cuboids by translating the sample. Here the $Cu_3Au(111)$ reflection is shown.

of the $200 \times 200 \times 13$ nm^3 cuboids arranged in a lithographic superlattice with periodicity $d_x = d_y = 400$ nm. This arrangement makes it possible to study simultaneously the phase transformation in the nano-structured area and in the thin film by a simple translation of the sample as shown in fig. 2(b). The actual X-ray scattering experiments have been performed at beamline C1 of the Hamburg Synchrotron Radiation Laboratory (HASYLAB) and at ID01 of the ESRF (Grenoble). Here we discuss the results obtained at beamline ID01. The X-ray source is a 42 pole undulator followed by a Si(111) monochromator, selecting a fixed energy of 14.0 keV, and two mirrors. The transverse X-ray coherence is determined mainly by the collimation of the beam between the sample and the detector. The different collimation conditions in the x- and z-directions perpendicular to the beam give rise to two transverse coherence lengths [17, 18],

$$\xi_{x,z}^{(t)} = \frac{\lambda}{\Delta\varepsilon_{x,z}} = \left\{ \begin{array}{ll} 50 \text{ nm}, & x \\ 50 \text{ nm–}180 \text{ nm}, & z \end{array} \right\}, \tag{2}$$

where $\Delta\varepsilon_{x,z}$ is the beam divergence in the x- and z-directions and λ the X-ray wavelength. In order to control the effect of the coherence length $\xi_z^{(t)}$ on the recorded diffraction patterns, $\xi_z^{(t)}(= 50\text{–}180)$ nm is scanned by varying the detector aperture. Note that the effective coherence length at the sample surface is increased by a projection effect leading to $\xi_{z_{\text{eff}}}^{(t)} = \frac{\xi_z^{(t)}}{\sin\theta}$ for an incident angle θ.

We now focus on the coherent diffraction phenomena. Typical experimental results for the $Cu_3Au(111)$ fundamental (fcc) reflection are shown in fig. 3 revealing pronounced interference patterns on top of a Lorentzian envelope. For a quantitative understanding of these diffraction patterns, it is necessary to sort out the different length scales involved in this problem, *i.e.* the X-ray wavelength $\lambda = 0.0886$ nm, the Cu_3Au lattice constant $a_0 = 0.373$ nm, the observed Cu_3Au grain size $b_x = 50$ nm, the size of the nano-cuboids $M_x a_x = M_y a_y = 200$ nm, $M_z a_z = 13$ nm, the lithographic lattice constant $d_{x,y} = 400$ nm and the 2D coherence volume given by $\xi_x^{(t)} \cdot \frac{\xi_z^{(t)}}{\sin\Theta}$ as illustrated in fig. 4. The associated kinematic X-ray diffraction amplitude then reads

$$I(\vec{q}) = I_0 \left[\sum_{n_x=0}^{N_x-1} e^{in_x q_x d_x} \sum_{n_y=0}^{N_y-1} e^{in_y q_y d_y} \frac{1}{(w_x^2+4q_x^2)} \frac{1}{(w_y^2+4q_y^2)} \sum_{m_z=0}^{M_z-1} e^{im_z q_z a_z} F(\vec{q})^2 \right]^2 + \tilde{I}(\vec{q}), \tag{3}$$

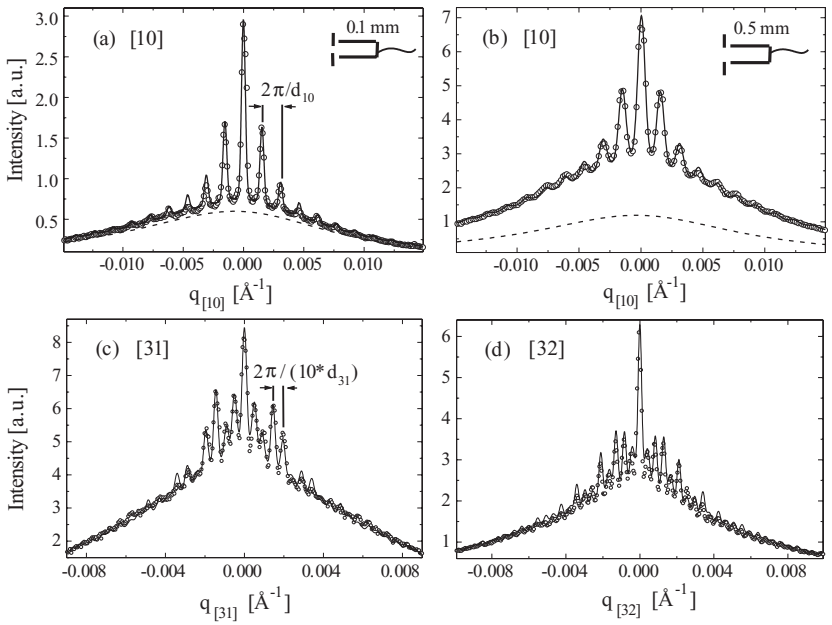

Fig. 3 – X-ray intensity distribution around the $Cu_3Au(111)$ reflection as measured from the Cu_3Au nano-cuboids for various conditions: (a), (b) incidence vector $\vec{k}_i$ in the [10]-direction and different detector slits (0.1 mm and 0.5 mm, respectively); (c), (d) incidence vector $\vec{k}_i$ in the [31]- and [32]-direction, respectively (see also fig. 2(a) and fig. 4).

where $n_{x(y)}$ is the summation over the number of nano-cuboids with superlattice spacing $d_{x(y)}$ in the $x\,(y)$-direction, m_z the summation over the number of unit cells within one nano-cuboid in vertical direction. $q_{x,y,z}$ are the coordinates of the reduced lattice vector. Notice that the mosaic block size is smaller than the lateral extension of one cuboid, thus the coherent summation over the number of unit cells in x- and y- direction is replaced by the Lorentzian line shape (1). $\tilde{I}\,(\vec{q})$ is a Bragg intensity contribution caused by imperfections in the lithographic superlattice (dashed curves in fig. 3). Considering only x- and y-directions, the lattice sums in (3) can be evaluated in a straightforward way yielding

$$I\,(\vec{q}) \propto I_0 \left[\frac{\sin^2\left(\frac{q_x}{2}d_x N_x\right)}{\sin^2\left(\frac{q_x}{2}d_x\right)}\frac{1}{\left(w_x^2+4q_x^2\right)}\right] * G(x) \left[\frac{\sin^2\left(\frac{q_y}{2}d_y N_y\right)}{\sin^2\left(\frac{q_y}{2}d_y\right)}\frac{1}{\left(w_y^2+4q_y^2\right)}\right] * G(y) + \tilde{I}\,(\vec{q})\,. \quad (4)$$

$*G(x)$ and $*G(y)$ denote convolutions with the associated coherence lengths in the x- and y-directions, respectively. A fit to the data with eq. (4) is included in figs. 3(a)-(d).

The inspection of the in-plane scans of the $Cu_3Au(111)$ reflection in the [10], [31] and [32] superlattice directions shown in fig. 3(a)-(d) reveals striking differences in the periodicity of the superlattice oscillations. This interference phenomenon is a direct consequence of the highly anisotropic transverse coherence volume of the X-ray beam, as illustrated in more detail in fig. 4 for two different situations, $\vec{k}_i$ being along the [10]-direction (fig. 4(a)) and along the [31]-direction (fig. 4(b)). The associated effective coherence volume $\frac{\xi_x^{(t)}\xi_z^{(t)}}{\sin\theta}$ (rectangular box) illuminates all nano-cuboids (drawn in black) which contribute to the coherent interference pattern observed in fig. 3 (1st term in eq. (4)). The nano-cuboids drawn in grey are partially illuminated by the coherence volume and give rise to the beat-like modulation in fig. 3. In

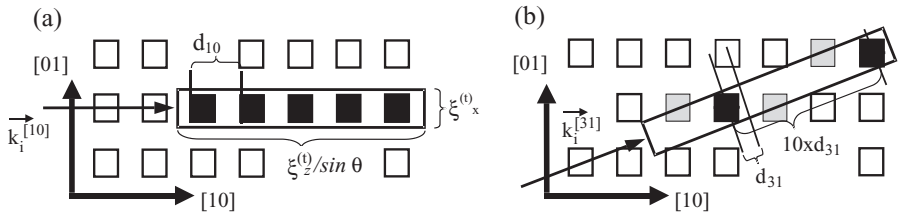

Fig. 4 – Illustration of the anisotropic coherence volume at the sample surface (see text).

turn, the dominating periodicity of the interference pattern in fig. 3(a)-(b) originates from the lithographic spacing $d_{10} = 400$ nm and from a significantly larger spacing ($10 \cdot d_{31} = 1265$ nm) in fig. 3(c). A similar argument holds for the [32]-direction in fig. 3(d). By taking these coherence phenomena properly into account, excellent quantitative fits can be obtained (full lines in figs. 3(c) and (d)). From the fitting parameters, we obtain information on the perfection of the 2D periodicity of the nano-cuboids which we can accurately control during the temperature-dependent studies as monitor for structural changes within and between the nano-cuboids.

We now turn to the *in situ* X-ray study of the order-disorder transformation within the Cu_3Au nano-cuboids. The sample was mounted in a UHV chamber with a Be window, a heater, and a temperature control via a thermocouple that was spring loaded to the backside of the sample. The $L1_2$ order-related (001) superstructure reflection from the nano-cuboids and from the thin film has been studied in parallel at the same sample (by translating the sample) as a function of temperature between room temperature and 670 K with a relative accuracy of 0.1 K. The temperature was raised to 640 K within 24 hours. The results are shown in figs. 5(a) and (b) along with the Cu_3Au(002) fundamental reflections in (d).

Figure 5(a) shows the (001) superstructure raw data as observed in the thin film area of the sample. One finds that the $L1_2$ long-range order decays with temperature and disappears at a temperature of around $T_c^{\mathrm{film}} = 660$ K (full symbols in fig. 5(c)) which compares well with the known bulk transition temperature. A rather different and quite unexpected observation is, however, found for the sample area containing the nano-cuboids as shown in fig. 5(b). Here the superlattice intensity undergoes a rather steep drop to zero at a much lower temperature $T_c^{\mathrm{cuboids}} = 460$ K (open symbols in fig. 5(c)) which is about 200 K lower than the bulk and thin-film transition temperature. (An incomplete cooling run confirmed those observations.)

In parallel, we investigated the temperature behaviour of the (002) fundamental fcc reflections within the thin film and the nano-cuboid area; the latter is shown in fig. 5(d). Apart from thermal expansion, we did not observe any change during the temperature treatment (in particular the interference fringes from the lithographic patterning did not exhibit any observable change) implying that the crystal structure within the nano-cuboids and the entire lithographic area stays intact during the entire experiment. Both the strongly altered characteristics of the temperature dependence of the order parameter within the nano-cuboids as well as the dramatic change in the transition temperature are very difficult to reconcile with our current understanding of surface and confinement effects upon first-order phase transitions [6, 7]: Surface effects, *i.e.* surface-induced disorder [9, 11] and surface segregation [12] in this system are found in a rather small surface area only (typically smaller than 100 Å). Finite-size effects can thus be ruled out. In fact, in a microscopy study of unsuspended Cu_3Au nano-particles, a decrease in the transition temperature was only found for a particle size below 100 Å [19, 20]. The characteristic feature in our nano-structured sample is the epitaxial

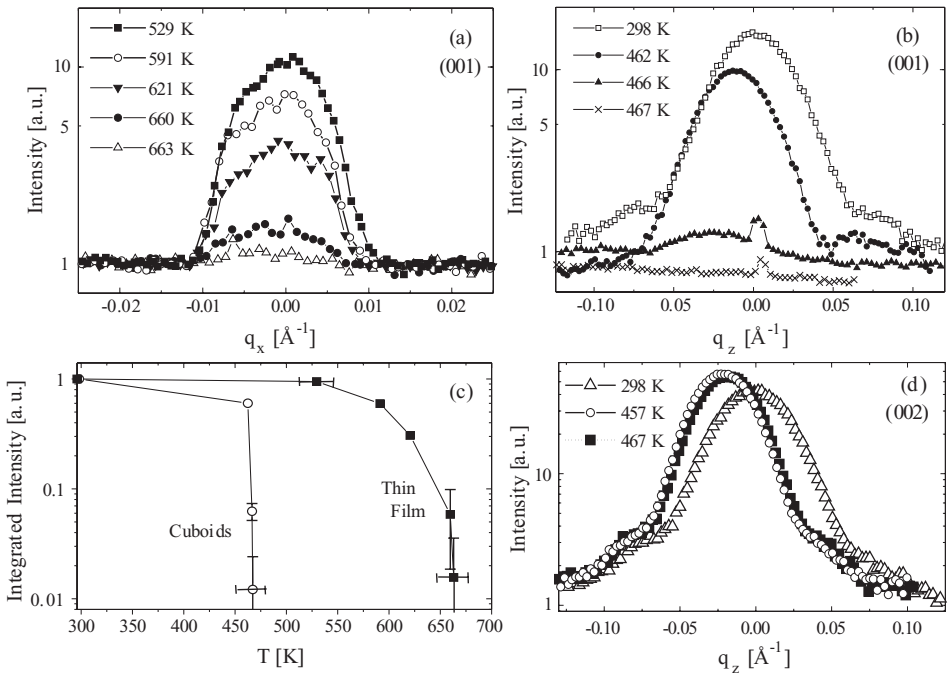

Fig. 5 – Temperature dependence of the $Cu_3Au(001)$ superstructure reflection of (a) the thin film and (b) the nano-cuboids. (c) Integrated intensity of the $Cu_3Au(001)$ superstructure reflection of the cuboids (open circles) and the thin film (full squares). (d) (002) fundamental reflection of the nano-cuboids for various temperatures.

relation of the binary nano-cuboids with the underlying Nb buffer. Our observations must therefore be intimately related to epitaxial effects acting on binary nano-structures. An obvious agent is epitaxial strain: The fcc-bcc epitaxial growth of $Cu_3Au(111)$ on Nb(110) is of Nishiyama-Wassermann type [21]. In turn, a strain-free growth would be possible for an fcc-film with a native lattice constant of $a^*_{\rm fcc} = a_{\rm bcc}\frac{\sqrt{3}}{2} = 3.81$ Å with $a_{\rm bcc} = 3.30$ Å for Nb. Thus, Cu_3Au ($a_0 = 3.73$ Å) grows with a tensile lattice mismatch of 2.2% giving rise to a noticeable strain in the system. Since this lattice mismatch is present in the film as well as in the nano-structures, it is rather puzzling why the $L1_2$-A_2 phase transition is so drastically altered only in the nano-structures. One may speculate whether the increased freedom in elastic relaxation within the nano-structures does allow extended composition profiles to enter the scenario to compensate the strain profile. Notice that a mismatch-free growth of $Cu_{1-x}Au_x$ is achieved for a lattice parameter of $a^*_{\rm fcc} = 3.81$ Å associated with a Au concentration of $x = 0.42$ at the Nb/Cu-Au interface which necessarily (because of the limited reservoir) would lead to a strong decrease of the Au concentration in the other parts of the nano-cuboid. This hypothesis that extended concentration profiles within the nano-cuboids would emerge could, in fact, alter the entire phase diagram. In order to critically test these ideas, we suggest careful measurements of the composition profiles *vs.* temperature as well as detailed theoretical calculations of the phase stability of the $L1_2$ phase in the presence of strain-induced concentration profiles within epitaxial Cu-Au nano-particles.

In summary, we have presented a first synchrotron X-ray study of the structure and the behaviour of the $L1_2$-A_2 phase transition of an epitaxial nano-structured Cu_3Au array con-

sisting of $200 \times 200 \times 13$ nm^3 cuboids. We have shown that the various length scales which are present in the sample and in the synchrotron beam give rise to strong interference phenomena which can be understood on a quantitative level. A first *in situ* study of the temperature dependence of the long-range order within the binary nano-cuboids reveals a rather dramatic reduction in the phase transition temperature in the nano-cuboids as compared to a closed thin film of the same thickness. We argue that this phenomenon cannot be explained by existing theoretical models but is most likely due to an extended composition profile which is sparked by the epitaxial strain at the Nb/Cu_3Au interface.

* * *

It is a pleasure to thank the technical staff at the IFW Dresden for their valuable help during the sample preparation, A. Mazuelas and T. H. Metzger with their technical group from ID01 at the ESRF as well as B. Adams from C1 at the HASYLAB for their helpful support during the X-ray experiments. We also would like to thank F. Livet and V. Bugaev for their very fruitful discussions.

REFERENCES

[1] Diaz-Ortiz A., Sanchez J. M. and Moran-Lopez J. L., *Phys. Rev. Lett.*, **81** (1998) 1146.
[2] Diaz-Ortiz A. and Sanchez J. M., *Phys. Rev. B*, **62** (2000) 1148.
[3] Borrmann P., Mülken O. and Harting J., *Phys. Rev. Lett.*, **84** (2000) 3511.
[4] Sosa-Hernández E. M., Aguilera-Granja F. and Morán-López J. L., *Phys. Rev. B*, **52** (1995) 5392.
[5] Nakanishi H. and Fisher M. E., *J. Chem. Phys.*, **78** (1983) 3279.
[6] Diehl H. W., *Phase Transitions and Critical Phenomena*, edited by Domb C. and Lebowitz J. L., Vol. **10** (Academic Press, London) 1986, p. 75.
[7] Binder K., *Phase Transitions and Critical Phenomena*, edited by Domb C. and Lebowitz J. L., Vol. **8** (Academic Press, London) 1983, p. 1.
[8] Dosch H., *Critical Phenomena at Surfaces and Interfaces* (Springer-Verlag, Berlin) 1992.
[9] Ern C., Donner W., Dosch H., Adams B. and Nowikow D., *Phys. Rev. Lett.*, **85** (2000) 1926.
[10] Mailänder L., Dosch H., Peisl J. and Johnson R. L., *Phys. Rev. Lett.*, **64** (1990) 2527.
[11] Dosch H., Mailänder L., Lied A., Peisl J., Grey F., Johnson R. L. and Krummacher S., *Phys. Rev. Lett.*, **60** (1988) 2382.
[12] Reichert H. and Dosch H., *Surf. Sci.*, **345** (1996) 27.
[13] Reichert H., Eng P. J., Dosch H. and Robinson I. K., *Phys. Rev. Lett.*, **78** (1997) 3475.
[14] Reinhard L. and Moss S. C., *Ultramicroscopy*, **52** (1993) 223.
[15] Wolverton C., Ozolins V. and Zunger A., *Phys. Rev. B*, **57** (1998) 4332.
[16] Vartanyants I., Ern C., Donner W., Dosch H. and Caliebe W., *Appl. Phys. Lett.*, **77** (2001) 3929.
[17] Holý V., Pietsch U. and Baumbach T., *High Resolution X-Ray Scattering from Thin Films and Multilayers* (Springer-Verlag, Berlin) 1999, p. 28.
[18] Brauer S., Stephenson G. B., Sutton M., Brüning R., Dufresne E., Mochrie S. G. J., Grübel G., Als-Nielsen J. and Abernathy D. L., *Phys. Rev. Lett.*, **74** (1995) 2010.
[19] Tadaki T., Koreeda A., Nakata Y. and Kinoshita T., *Surf. Rev. Lett.*, **3** (1996) 65.
[20] Tadaki T., Kinoshita T., Nakata Y., Ohkuba T. and Hirotsu Y., *Z. Phys. D*, **40** (1997) 493.
[21] Hellwig O., Theis-Bröhl K., Wilhelmi G., Stierle A. and Zabel H., *Surf. Sci.*, **398** (1998) 379.